J. theor. Biol. (1976) **59**, 443–466

Tree Structures: Deducing the Principle of Mechanical Design

THOMAS A. MCMAHON

AND

RICHARD E. KRONAUER

Division of Engineering and Applied Physics, Harvard University, Cambridge, Massachusetts 02138, *U.S.A.*

(*Received* 21 *March* 1975, *and in revised form* 6 *October* 1975)

A statistical description of the branching patterns of trees is proposed in the context of a power-law tapered beam model. Depending on the exponent which describes tapering of the depth of the beam, the model either preserves geometric, elastic, or static stress similarity. A detailed study of the morphometry of three oak, one poplar, one cherry, and one white pine corroborates the stationarity of these branching structures and fits the elastically similar model. A separate study of the natural frequencies of branch segments and whole trees within four species also agrees with the predictions of the elastically similar model.

1. List of Symbols

N = number of segments in a particular order.
n = order number.
T = links in order one.
R_B = branching ratio, average $N(n)/N(n+1)$.
R_D = diameter ratio, $\bar{d}(n+1)/\bar{d}(n)$.
d, $\bar{d}$ = diameter of a link, average diameter within an order.
s = distance from virtual origin in power-law model.
h = depth of doubly tapered power-law beam.
b = breadth of doubly tapered beam.
β = power of depth taper, Fig. 2.
α = power of breadth taper, Fig. 2.
λ = overall length of beam, from built-in end to virtual origin.
Δ = deflection of the tip due to loading by the beam's own weight.
f_n = natural frequency in lowest mode of vibration.
ω = $2\pi f_n$, angular natural frequency.

l_0 = length between virtual origin and cutoff point.
l_{max} = distance from the clamp to the tip of the longest branch in the frequency–length measurements.
L_i = average path length, equation (1).
l_{ij} = a single path length.
e_i = number of first-order endings served by a link i.
ρ = mass density.
E = elastic modulus, slope of stress–strain curve.
r = correlation coefficient.
θ_1, θ_2 = chord angles, Fig. 8.

2. Introduction

It is a popular notion that trees occurring in nature have evolved branching patterns which perform their task in some optimal way, but the principle of optimality which is presumably the principle of their mechanical design has yet to be discovered. Geomorphologists interested in river patterns pioneered the application of quantitative methods to branching networks only relatively recently. Although Gravelius (1914, quoted by Woldenberg, 1968) applied the concept of ordering to a river network by assigning a heirarchy of integers to the various links (a link is a connecting element between two nodes), his aim was to identify the orders according to the historical development of the river, labeling the original main trunk as first order and later streams as higher order. Woldenberg points out that rivers labeled by this system have totally different values for order applied to branches of equivalent size.

Horton (1945) introduced an ordering scheme which provided better correlation between order number and stream size. Under Horton's scheme, two separate operations are required to assign the final order number. In the first operation, all terminal links are assigned order number 1, and when first-order links meet they form a link of order 2. For convenience, and without loss of generality, each branching is assumed to be dichotomous. When two daughters of different order meet, the resulting parent takes the same order as the higher of the two joining links. Thus a 3 and a 2 merge to give a 3, as do a 3 and a 1, but a 3 and a 3 merge to give a 4 [Fig. 1(a)]. In the second operation, many of the order numbers are changed. Starting with the main trunk, a path is traced to a terminal link choosing the larger order number at each junction. At a junction where daughters of equal order meet, one is arbitrarily chosen over the other to continue the path. This path retains the same order number as the main trunk. The procedure is repeated for streams of the next-highest order, and so on down to second-order links

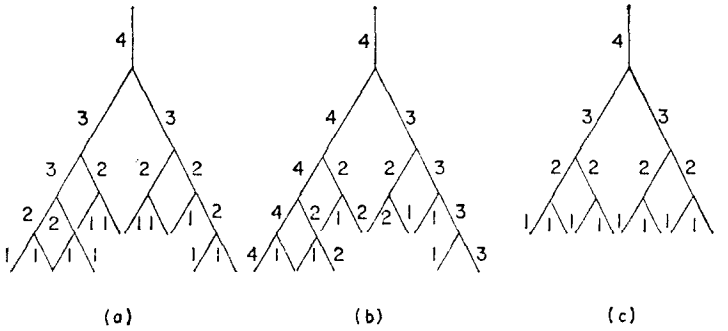

FIG. 1. Ordering and symmetry. (a) Horton's first operation, which is identical to Strahler ordering, provided that all contiguous links of a given Strahler order are counted as a single segment. Thus there is one segment of order 4, 2 segments of order 3, 5 segments of order 2, and 11 segments of order 1 in the figure. (b) Horton's second operation. (c) A symmetric branching pattern, in which the Strahler order number changes at each node.

[Fig. 1(b)]. Contiguous links of the same order are counted as one segment. Horton found that when a river is ordered this way, there is a linear relation between order number and the logarithm of population of segments of that order. Horton's method is subject to the same objection raised earlier for Gravelius', that streams of like magnitude may have a different order number.

Strahler (1953) suggested the modification that only the first operation of Horton's method should be used, with no reclassification. Strahler's method has been useful for describing not only rivers, but the bronchial tree and pulmonary arteries (Cumming, Henderson, Horsfield & Singhal, 1969; Parker, Horsfield & Cumming, 1971; Woldenberg *et al.*, 1970) bile ducts in the liver (Woldenberg, 1968) and botanical trees (Holland, 1969; Barker, Cumming & Horsfield, 1973). One of us has previously published a popular account of much of the substance of the present paper, including the application of Strahler ordering to trees (McMahon, 1975).

A symmetric branching pattern is one in which the Strahler order changes at each node [Fig. 1(c)]. In such a pattern, the number of segments is given by $N = 2T(2)^{-n}$, where T is the total number of segments of order 1. Thus $\log N = \log 2T - n \log 2$, so that the slope of a plot of $\log N$ vs. n is a negative number, the antilog of whose absolute value (in this case 2) is the branching ratio R_B, the average factor by which the population of order n exceeds that of order $n+1$. The best straight line fit of $\log N$ vs. n defines the branching ratio even for asymmetric structures, as in Fig. 1(a). In Strahler ordering, the branching ratio may not be less than 2, but may be any higher number, where the degree of asymmetry (the "depth" of the

structure) increases with R_B. Similarly, the mean diameter of branches in any order plotted vs. order number of a semilog plot yields the diameter ratio R_D as the antilog of the slope, which may possibly be the same between all orders.

Horsfield (1967) has suggested still another consistent ordering scheme. The Horsfield order of the parent is always one greater than the greatest order of the two daughters. Thus the Strahler and Horsfield schemes are identical for symmetric branching but the same asymmetric structure has a greater number of Horsfield orders than Strahler orders. Horsfield (1972) has investigated the relative merits of both ordering schemes and concluded that the Strahler method is to be preferred in many situations, since in markedly asymmetrical systems, Horsfield ordering may not give a straight line relation between $\log N$ and n because of the necessity of changing the order of the main trunk whenever it is joined by the slightest twig.

In this paper, we shall be seeking the optimality principle by which botanical trees may be said to be designed. This purpose requires us to be aware not only of the topology of the tree but of the actual length and diameter of each link, since these determine the stiffness, strength, and also the load which the limbs must bear at any point within their structure. Thus the concept of order number will be augmented by a new descriptor, the average distance along a branch from the twigs, which has the dimensions of length. However, when we do invoke the concept of order number we will be using the Strahler system.

3. Optimality Principles and Structural Models

It is possible to suggest models for optimal branching structures which do not make use of the concept of order number at all. Consider the tapered cantilever beam of rectangular cross-section in Fig. 2(a) and (b). The depth h and width b taper with length s from the virtual origin according to power-law rules $h = k_1 s^{\alpha}$, $b = k_2 s^{\beta}$. This beam represents a limb growing out from the trunk of a tree, or even the whole tree itself. It may be shown that cuts made on the dotted lines in the plan view of Fig. 2(a) do not change the deflection of the structure under its own weight. The self-loaded unbranched beam (before cutting) is statically and dynamically the same as the branched beam (after the cuts have been made). The cuts may be spread uniformly to give the branching structure in Fig. 2(e) without changing this conclusion. One may also derive (Appendix A) that if the structure is elastically self-similar (i.e. the deflection of the tip, Δ, divided by the overall length, λ, is a constant, however much λ may vary), then $\beta = \frac{3}{2}$, whatever the value of α. As an alternative hypothesis, if the stress in the fibers at the top and bottom

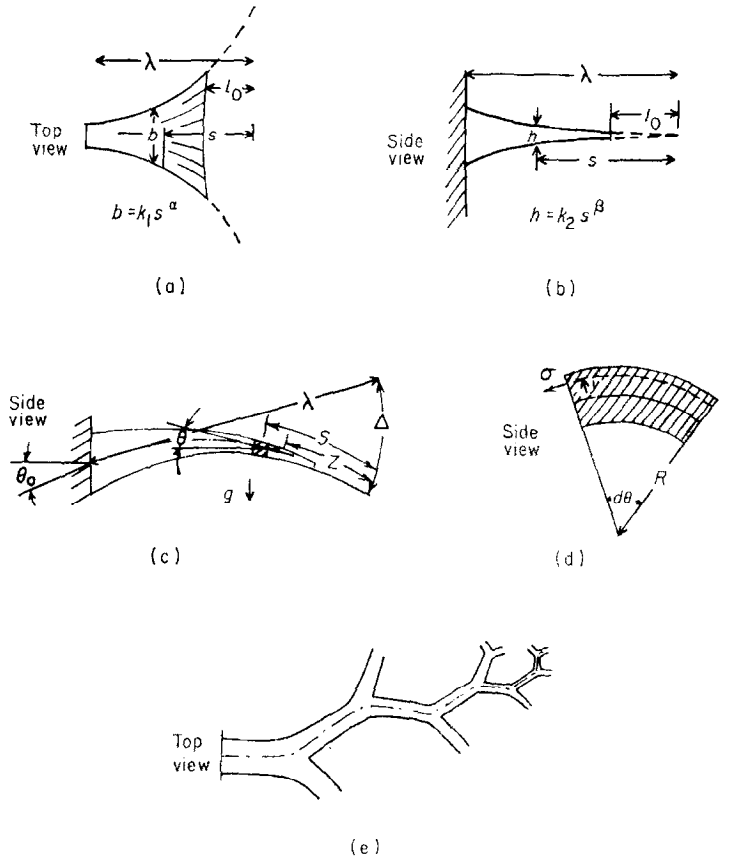

FIG. 2. Tapered power-law beam model. (a) Top view, showing how the breadth b tapers according to $b = k_1 s^{\alpha}$. (b) Side view, showing how depth h tapers according to $h = k_2 s^{\beta}$. (c) Side view showing how the weight acts to produce a tip deflection Δ. (d) The shaded element in part (c) redrawn to a larger scale, showing the stress σ acting at a distance y from the neutral axis. (e) Top view of the beam, showing how the cuts made in (a) may be separated to give a tree structure.

surfaces of the beam are to be kept the same over the entire length, then $\beta = 2$, provided the deflections are small, again independently of the choice for α (Appendix A2).

In what follows, we will examine morphometric data from several tree species in an effort to determine which, if any, power-law model gives a successful description of the true structure. We will be aided by an observation which is simple to make in the field, the natural frequency in the lowest mode of bending. As shown in Appendix B1, the beam tapered to insure elastic similarity ($\beta = \frac{3}{2}$) has a natural frequency f_n proportional to $\lambda^{-\frac{1}{2}}$.

This stands in contrast to the geometrically similar tapered beam ($\beta = 1$), where $f_n \propto \lambda^{-1}$, the uniform-stress tapered beam $\beta = 2$), where f_n is independent of λ, and the untapered beam ($\beta = 0$) where f_n is proportional to λ^{-2}.

4. Branching as a Random Process

Before comparing the deterministic models of the previous paragraph with actual trees, it is reasonable to ask how randomness found in nature fits into the discussion. Trees develop their branching structures as the result of the three interacting processes of bifurcation (sprouting), growth (in length and diameter) and death (self pruning). Without a study of the time history of development, a statistical description of this randomness cannot be had. However, an instantaneous view of the structure at one time does permit a statistical description of the way in which the several dynamic processes have interacted up to that time. If this combined random process is stationary, a comparison of two trees of different size (in the same physiologic condition), or two regions in the same tree should give the same statistical branching rules. It is this hope which appears to have motivated all the previous originators of ordering schemes, since stationarity is implicit in the concept of a single branching ratio throughout a tree.

There exists extensive evidence supporting the argument for stationarity. In three species of mallee Eucalyptus, Holland (1969) examined trees between 2 and 20 years of age and found R_B independent of age. Oohata & Shidei (1971) found a stable value for the R_B of 7-year old *Quercus phillyraeoides*, despite large controlled differences in density of planting and light intensity levels. In several species of both evergreen and deciduous trees, they found R_B fixed for a species, although the evergreens have a consistently higher R_B (near 5·0) than deciduous trees (near 3·0). Leopold (1971), found a constant R_B throughout the orders of a 12-year old fir (*Abies concolor*), two ash (*Fraxinus* sp.) and a small tulip (*Liriodendron tulipifera*). Barker *et al.* (1973) found constant R_B within an apple and a birch tree, although the R_B's for the two species were different. Horsfield (1972) grew tree patterns on a computer by employing certain rules guiding random number generators and found R_B a constant within any completed pattern, although R_B could be different between two patterns grown under different rules.

Does the very fact that R_B is found to be a constant within a given tree have something to do with optimality or the principle of its mechanical design? No, as Horsfield's computer-grown trees demonstrate—this is a property of all random branching patterns. Does the particular value of R_B within a tree have to do with its mechanical design? No again, or every species would be seen to be optimizing itself according to a different principle. We

suggest that R_B in a species is directed in part by some mechanism, perhaps genetic, which is entirely unrelated to the optimality principle which decides the mechanical proportions (i.e., statistically independent). It is as if all trees started as the same blank doubly-tapered beam in Fig. 2(a) and the choice for α and cuts were made in such a way as to produce a high R_B in some species and a low R_B in others. Note that R_B, and thus the "depth" of the structure, increase as α decreases. A direct correlation between α and R_B is not easy to make because the Strahler system is not "continuous", i.e., links of adjacent order do not necessarily touch one another. The point to be remembered here is that α, and thus R_B, according to the tapered-beam model, are independent of the principle of mechanical design, but since β represents that principle, we should not be surprised to find β the same in trees of very different outward appearance.

5. Methods and Procedures

The length and midpoint diameter of each quasi-cylindrical link of one poplar, three oak, one cherry, and one white pine were measured. The measurements necessarily began at the tips of the twigs, not at the virtual origin where the h dimension, or diameter of the twig, is zero [Fig. 2(b)]. Only live branches were considered; all dead structures were removed before measuring began. The first-order links (twigs) were all found to be about the same diameter in a given species. This observation facilitates comparison with the power-law models, since at the cutoff point $s = l_0$ in Fig. 2(a), one would expect the diameter [given by $h(l_0)$] to be roughly constant. The red oak was such a large tree that we had to discontinue measurement for branches less than 1 cm in diameter. This had the effect of increasing l_0 by a large factor without otherwise influencing the measurements.

The only criterion applied to selection of the trees was that they be found standing reasonably alone. The trees were felled for convenience in making the measurements. Following the convention established by Horsfield & Cumming (1968), we assigned each link an arbitrary identification number, and recorded this number along with the number of its parent, its length, and its diameter at the midpoint. The data were processed by a computer program which was able to recreate most of the topological details of the tree. The tree specimens are identified in detail in Table 1.

As a separate study, we measured the natural frequency in a series of limbs of different length and in whole trees of three species. After securing the limb with a bench vice at the desired length, the distance l_{max} to the extreme tip of the limb was measured, and the limb was manually excited in its lowest mode of vibration. The frequency was obtained by counting the

TABLE 1

Identification of the specimens whose morphometrics were studied. The parameter l_0 was computed by fitting the length-diameter data to the power-law model. Since the red oak measurements excluded branches less than 1 cm in diameter, it was possible only to assign provisional orders to each link

Genus	Species	Common name	Total links	Base diameter (mm)	Total height (mm)	R_B	(r)	R_D	(r)	l_0 (mm)
Quercus	*rubra*	Red oak	1362	203·0	13776	3·83	(0·996)	1·56	(0·955)	1750 (including truncation)
Quercus	*alba*	White oak	3325	96·1	4385	4·37	(0·999)	1·88	(0·996)	217
Quercus	*alba*	White oak	2630	84·4	2847	4·11	(0·999)	1·84	(0·997)	112
Populus	*tremuloides*	Poplar	1945	190·0	5357	4·22	(0·995)	1·86	(0·996)	No convergence
Prunus	*Pennsylvanica*	Pin cherry	289	30·0	1472	5·18	(0·999)	2·05	(0·999)	113
Pinus	*strobus*	White pine	803	64·0	1986	4·44	(0·997)	2·04	(0·996)	55

number of cycles completed in a given time. The oscillations were restricted to a small enough amplitude so that doubling the amplitude had no effect on the natural frequency. Observations were made both before and after the leaves appeared during the spring, summer, and fall of 1974 on trees found near Ripton, Vermont, and Harvard, Massachusetts.

6. Results

If trees were perfectly symmetric branching structures, it would be a simple matter to compare them with the model in Fig. 2, since there would be an unambiguous length to the tip, $s-l_0$, associated with each diameter $h(s)$.

In dealing with the statistics of real trees, we choose to represent $h(s)$ by the local link diameter d_i, where i is the identification number. This link will service m end twigs, and each will have an associated length-to-tip l_{ij}, $1 \leq j \leq m$. We represent the effective length-to-tip as the average of these individual l_{ij}.

$$(s-l_0)_i = L_i = \frac{1}{m}\sum_{j=1}^{m} l_{ij} \tag{1}$$

In what follows we will use the expression "path length" to denote length-to-tip and it will be understood that path length includes the length of the local link.

The local diameter may be expected to correlate more successfully with this average path length L_i than with any single path length l_{ij}, since the path following a small branch joining the main trunk experiences a large change in both L_i and d_i at the junction, but only a small change in l_{ij}.

Stationarity

In a perfectly symmetric branching structure, ($R_B = 2$), all path lengths l_{ij} from link i leading to a first-order twig are equal, so a histogram showing the probability that a randomly selected path has a given normalized path length l_{ij}/L_i shows a sharp spike (δ-function) centered at $l_{ij}/L_i = 1{\cdot}0$.

Deviations from symmetry may be of two kinds. First, topological symmetry may be preserved, ($R_B = 2$) but the lengths and diameters of the individual links may vary in some random way. Second, the topology may vary randomly ($R_B > 2$). Both effects tend to broaden the probability histogram for path length. Notice that if the structure is statistically stationary throughout the tree then the shape of the normalized length histogram will be the same at any point in the tree.†

† To be more precise, a small length to the virtual origin must be added to both the individual path lengths, l_{ij}, and the average length, L_i, in the formation of the normalized histogram.

Figure 3 shows path length probability curves for the large white oak, the poplar, and the pine. The two curves in each part of the figure represent the ensemble average curve for a typical distal link (serving a small number of endings e_i) as opposed to a typical proximal link (serving a large number of endings). The two curves in each part are roughly the same shape, neither being more peaked nor more broad than the other. This is true despite the fact that the shapes of the curves in Fig. 3(c) are somewhat different from those in Fig. 3(a) and (b), since each species has its own characteristically shaped curve.

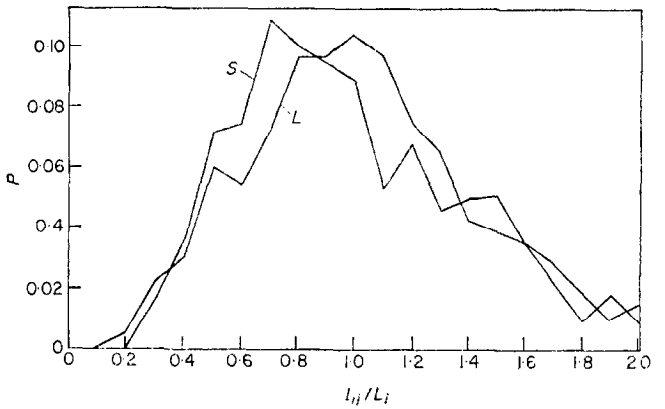

FIG. 3(a)

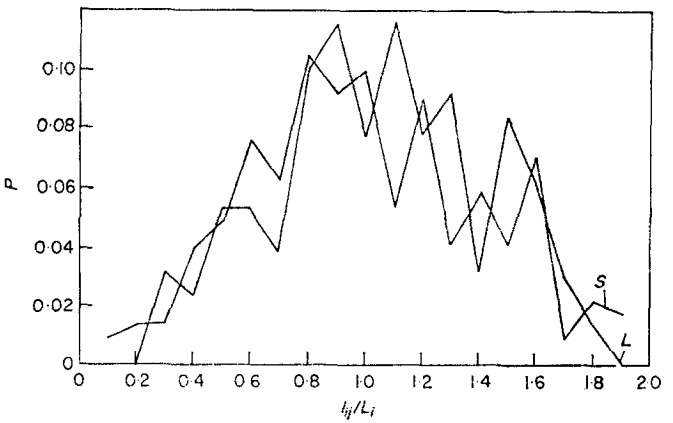

FIG. 3(b)

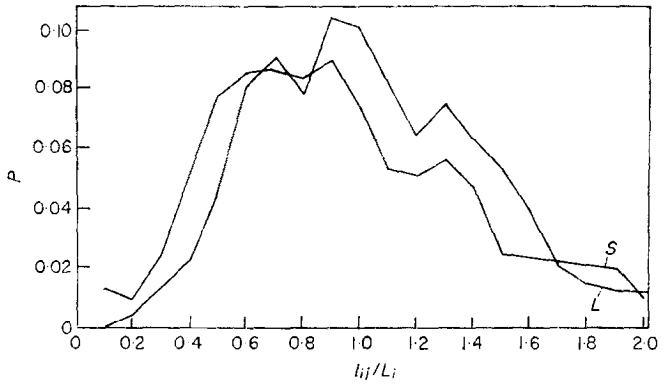

FIG. 3(c)

FIG. 3. Path length probability histograms. The probability that a given path from link i to a first-order termination has length l_{ij} is p. The abcissa is normalized with respect to the average length to the tip, L_i. The curves represent the ensemble average of path length probability histograms taken over all links in the tree whose number of endings served, e_i, falls within a given interval. (a) Large white oak: $16 \leq e_i \leq 20$ for the curve marked S, and $100 \leq e_i \leq 110$ for the curve marked L. (b) Poplar: $11 \leq e_i \leq 15$ for the curve S and $71 \leq e_i \leq 80$ for L. (c) White pine: $11 \leq e_i \leq 15$ for S and $51 \leq e_i \leq 60$ for L. Perfect stationarity of the branching structure implies that the S and L curves in each specimen are identical.

The number of segments in an order and the average diameter of segments in that order are summarized in Table 2 for the six specimens. The semi-log plots in Fig. 4 for the two white oaks of different size show almost identical branching ratios and radius ratios. The diameter plot shows that both oaks have nearly the same average diameter in each order up to the two highest orders where they diverge somewhat. This behavior would be expected if trees followed the power-law model developed earlier, since average diameter should be more closely correlated with $L_i + l_0$ than with order number. Order numbers are discrete whereas $L_i + l_0$ is continuous: as a tree grows larger, there are only a very few occasions when it increases its highest order number, even though it is continuously increasing its overall height. Thus the diameter-order plot in Fig. 4(b) would wag like a tail each time the tree grew large enough to add an extra order. The fixed base of the tail would be the mean line observed at low order numbers; the wagging would occur in the higher-order segment.

Optimality principle

In a previous paper, (McMahon, 1973), one of us has argued that trees generally limit their overall height to about $\frac{1}{4}$ the critical buckling height of a uniform cylinder of the same base diameter loaded under its own weight.

TABLE 2

Number of segments, N, *and average diameter,* d(*cm*), *in each Strahler order of six specimens studied. The red oak has only been provisionally ordered, as discussed in the text*

Specimen	Order 1		Order 2		Order 3		Order 4		Order 5		Order 6	
	N	$\bar{d}$	*N*	$\bar{d}$	*N*	$\bar{d}$	*N*	*d*	*N*	*d*	*N*	*d*
Red oak	674	1·38	163	2·83	44	5·62	12	9·99	2	9·05	1	13·98
Large white oak	1653	0·28	338	0·48	83	0·91	24	1·38	4	3·32	1	6·68
Small white oak	1312	0·27	316	0·47	83	0·88	25	1·43	5	2·78	1	6·15
Poplar	956	0·69	256	1·10	68	1·96	15	3·43	2	7·67	1	14·53
Pin cherry	144	0·25	23	0·53	5	1·06	1	2·13	—	—	—	—
White pine	402	0·32	111	0·56	30	1·04	6	2·59	1	5·22	—	—

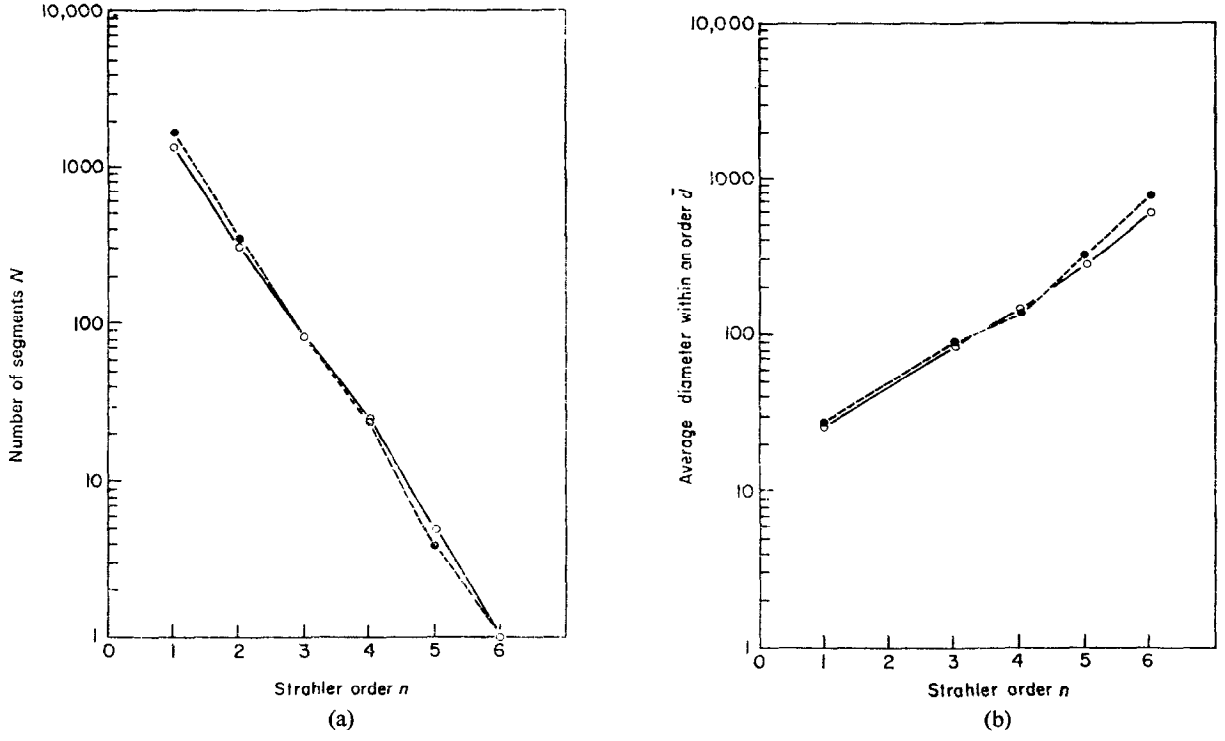

FIG. 4. (a) Number of segments N in each order vs. order number n for the white oaks. The branching ratio R_B is the average factor by which $N(n-1)$ exceeds $N(n)$. (b) Average diameter $\bar{d}$ within an order vs. order order number. The diameter ratio R_D is the average factor by which the diameter of order $n+1$ exceeds that of order n. - - - -, large white oak; ———, small white oak.

The line giving the proportions of such a critical cylinder, whose mechanical properties ρ, mass density, and E, elastic modulus, are appropriate for green pine, is shown in Fig. 5. The points represent the overall height and diameter 5 ft from the base of record specimens of more than 500 species of trees found in the U.S.A. To make the comparison valid, one depends on the approximate constancy of the ratio E/ρ in green woods, even though both

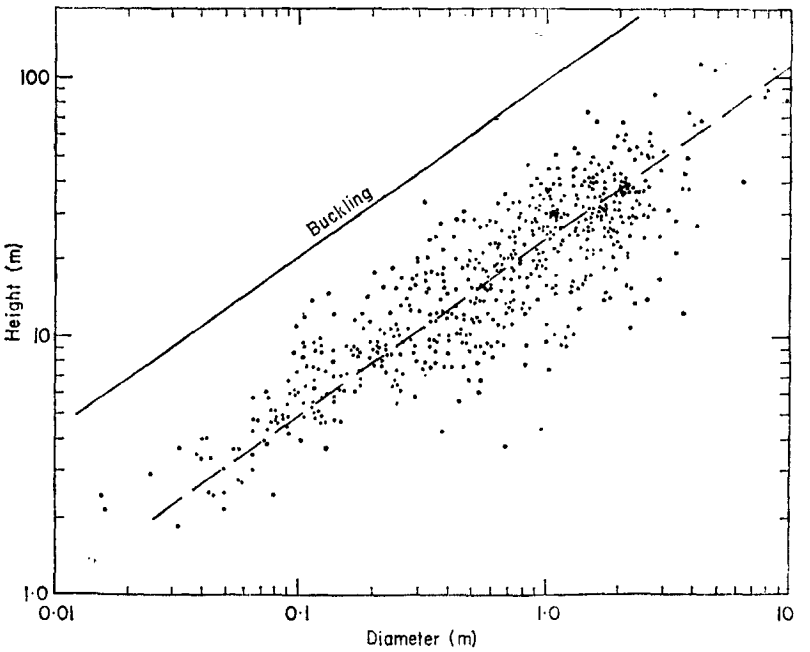

FIG. 5. Overall height vs. base diameter for 576 record trees representing nearly every species found in the United States. Data from the American Forestry Association's Social Register of Big Trees. The argument is that trunk proportions are limited by elastic buckling criteria, since no points lie to the left of the solid line (from McMahon, 1973).

E and ρ may vary from species to species. Both the solid line representing the uniform cylinder and the broken line drawn by eye through the center of the points have slope $\frac{2}{3}$ in the double-logarithmic plots. Thus elastic similarity is approximately maintained in comparisons of the overall proportions of small and large trees, even across species boundaries.

Figure 6 shows what happens when we make that same comparison of L against d within a single specimen, in this case the large white oak. We find for each path, as illustrated for the superposed data following 12 separate paths from a terminal twig to the trunk, that the points fall about a curved

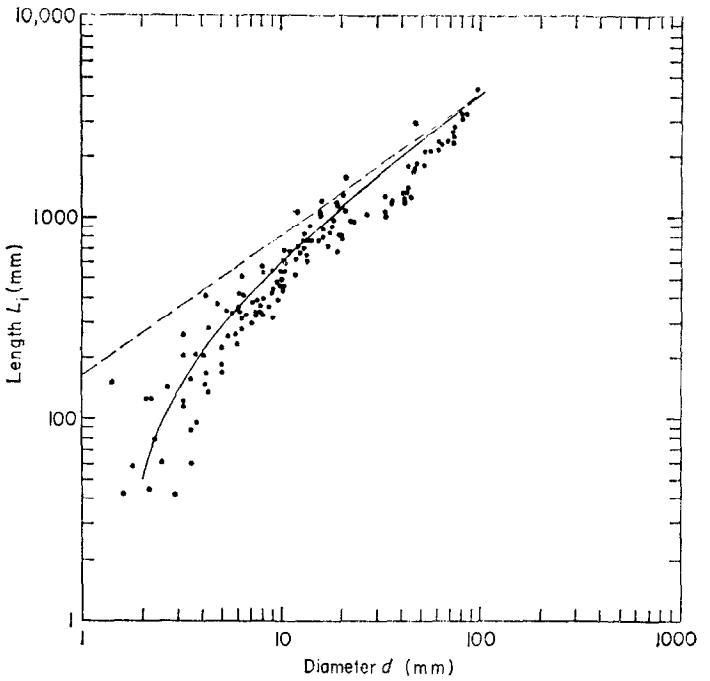

FIG. 6. Average length L_i vs. diameter d for 12 paths from a random twig to the base in the large white oak. The broken line is the best least-mean-squares fit for all possible twig-to-trunk paths in the entire tree, $L_i+l_0 = 166\ d^{0.71}$, with $l_0 = 217$ mm. When the length to the virtual origin l_0 is subtracted, the solid line shows L_i vs. d.

line in the log–log plot. This curved line becomes the straight broken line when L_i+l_0 instead of L_i is plotted against d, as expected. The computer algorithm chooses l_0 on the basis of a least-mean-squares power-law fit, iterating l_0 until the highest correlation coefficient is obtained. The data we start with thus yields three parameters when fitted to the power-law model: the intercept, the slope β, and the distance to the virtual origin l_0. The results of this procedure taken as an average over every path from a first-order twig to the trunk in each of the specimens is shown in Table 3. The exponent β is found to be $1{\cdot}50\pm0{\cdot}13$ for the specimens studied, in reasonable agreement with the model postulating elastic similarity. This procedure proved to be a rather insensitive test of the power law, since the correlation coefficient passed through only a very shallow maximum in the five cases where a maximum could be found. For example, the large oak data showed a correlation coefficient r of 0·967 for power $\beta = 1{\cdot}50$, while the maximum occurred for a choice of $\beta = 1{\cdot}41$ where r was 0·969.

TABLE 3

Predictions of the various similarity models with respect to taper exponent (β) and natural frequency (f_n), compared with experiments

Models	Depth taper exponent β, $d \propto \lambda^{\beta}$		Frequency-length exponent γ, $f_n \propto \lambda^{\gamma}$	
Geometric similarity	1·0		−1·0	
Elastic similarity	3/2		$-\frac{1}{2}$	
Static stress similarity	2		0	
No taper	0		−2	
Experiments				
White pine	1·37	average = 1·50		
Red oak	1·51			
Large white oak	1·41			
Small white oak	1·66			
Cherry	1·50			
AFA record specimens (Fig. 5)	1·50			
All poplars			−0·60	average = −0·59
All maples, leaves on			−0·63	
All maples, leaves off			−0·68	
All larches			−0·58	
All oaks, leaves on			−0·54	
All oaks, leaves off			−0·55	

The results of the studies of natural frequency f_n versus extreme length l_{max} are shown in Fig. 7. As discussed in Appendix 3, we can expect approximately the same result tabulating f_n against l_{max} as we would have found if it had been possible to tabulate f_n as a function of λ. Least-mean-squares power-law fits to the data are summarized in Table 3. This is quite a sensitive test of the power-law rule, as one may see by studying the table. Geometric similarity would require a slope of -1 in each of the frequency–length plots of Fig. 7, while constant stress similarity would require zero slope. Although the points in Fig. 7 show the inevitable scatter due to biological variation, both of these alternatives may be completely excluded. Again, the experiments clearly favor the elastically similar model over the alternatives, even though the average frequency–length exponent is $-0{\cdot}59$ instead of the predicted $-0{\cdot}50$.

In Fig. 7(a) and (b), points representing paths along the main trunk are differentiated from points representing paths along lateral branches. The natural frequency of a branched segment including the main trunk is consistently higher than that of a lateral branch of equal length.

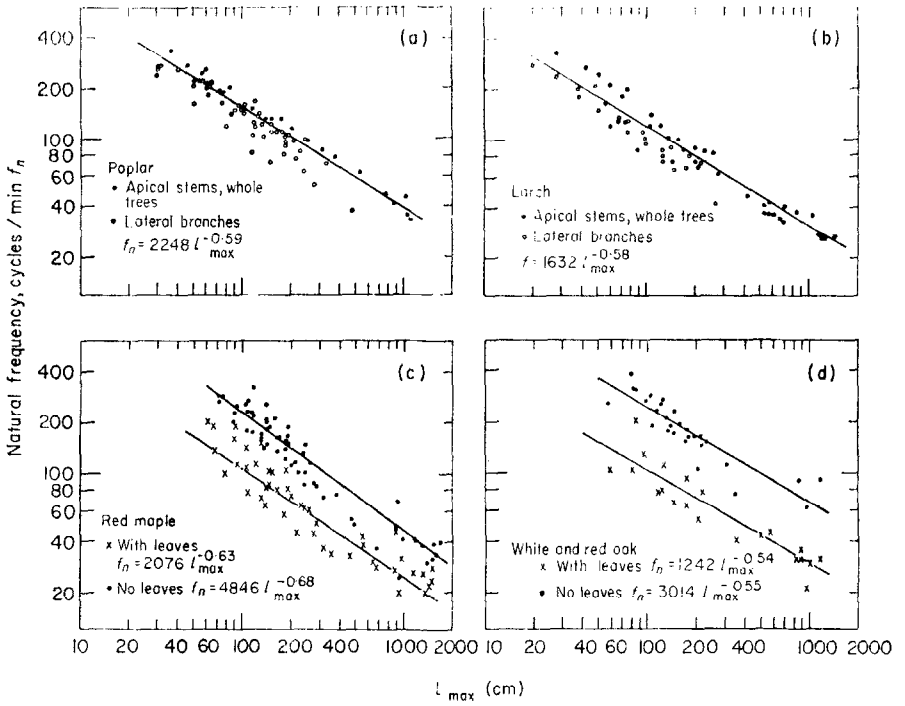

FIG. 7. Natural frequency vs. length for four species. (a) Poplar, (b) larch, (c) red maple, with and without leaves, (d) red and white oaks, with and without leaves.

The natural frequency showed very little sensitivity to the plane in which bending vibrations were excited. For example, a white oak 1454 cm in height had an f_n of 38 cycles/min for east–west bending and 40 cycles/min for north–south bending. In most trees, f_n in one plane was within 2% of f_n in the orthogonal plane. This is a demonstration of the mean radial symmetry of the crown shape and the trunk cross-sectional shape.

An oak or maple bearing full summer leaves had a natural frequency between two and three times lower than the same tree after leaf fall. In Fig. 7(c) and (d), maples and oaks with and without leaves are contrasted. The large factor by which the leaves lower the natural frequency of a tree is probably due to the fact that their damping and mass (plus the added mass of the air they entrain) is concentrated near the tip, where the amplitude of oscillation is largest. The weight of the leaves themselves was found to be only 30·5% of the total weight of an 85 cm white oak. This fraction would be smaller in larger trees.

7. Summary and Conclusions

Although the analysis of branching patterns has depended on the concept of integer ordering until the present time, it is clear that any scheme which does not keep track of the actual physical dimensions of a tree cannot investigate the principle of its mechanical design. We suggest here three doubly-tapered power-law models for branching structures and note that each implies a different design principle.

In a detailed study of the morphometry of six complete specimens representing five species, we find further evidence supporting the conviction expressed before in the literature that the branching pattern within any species is approximately stationary. This means that the structure is self-similar with respect to the parameters we recorded, so that any patch of the structure is a model of the entire tree. Hence, one branching ratio and one diameter ratio is good for the whole tree, even the whole species.

The morphometric studies also allowed us to determine which among the alternative power-law models provided the best description of real trees. In each of the specimens, the elastically similar model provided the best fit.

In an independent set of experiments, clamped branches and whole trees of four species were excited in their lowest modes of vibration. The natural frequencies of these vibrations were found to vary approximately inversely as the square root of the greatest length of the branch, again in agreement with the elastically similar model. This result was found true both in trees without leaves and in maple and oak trees bearing their full summer leaves. The natural frequencies were different by about a factor of 2·4 between trees with and without leaves.

Why should trees have decided to preserve elastic similarity in their branching structure? The question must stand as a subject for future research, but some speculation may not be out of place here. The overall proportions of the trunk must be robust enough to avoid buckling under its own weight, and this is surely the reason why none of the points in Fig. 5 fall to the left of the solid line. If the overall proportions of trees are set by genetic information, then perhaps this same information incidentally establishes the proportions of the limbs as well as the trunk.

A more dynamic hypothesis suggests that every tree is continually sensing its own overall geometry, altering its proportions in such a way as to keep that geometry stationary during growth. Holland (1969) found that the shape of the crown is invariant of age in mallee Eucalyptus. If Fig. 8 is schematic of a growing tree, the only way the crown shape could be maintained the same between a small and a large tree would be to keep the chord angles θ_1, θ_2 . . . the same. This requires that the tip deflection Δ divided by the

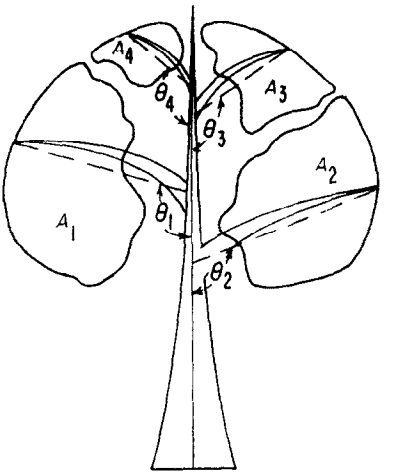

FIG. 8. Schematic of a growing tree loaded under its own weight. The limbs support the crown segments A_1, A_2, etc. Unless the chord angles θ_1, θ_2, . . . are maintained constant throughout growth, the crown segments might find themselves out of place in successively larger trees, and a species could not have a constant crown shape. Constancy of crown shape implies elastic similarity as the principle of mechanical design, as discussed in the text.

limb length λ be maintained constant, which is just the condition for elastic similarity. If this condition were not met, the crown segments A_1, A_2 . . . supported by each branch might find themselves out of place in successively larger trees, e.g. dragging on the ground or squashed together at the apex.

In conclusion, it now seems possible to state with some confidence that the principle of mechanical design within the tree species studied is the maintenance of elastic similarity. The mechanism which establishes this similarity is very much an open question, one whose ultimate answer promises subtle understanding of the nature of trees.

The authors wish to acknowledge the technical assistance of D. Bogen, R. Lundberg, P. Brockenstedt, T. Fly, D. Margolis, and W. Taffel. The work was supported in part by a grant from the Clark Fund, Harvard University and the Division of Engineering and Applied Physics, Harvard University.

REFERENCES

BARKER, S. B., CUMMING, G. & HORSFIELD, K. (1973). *J. theor. Biol.* **40**, 33.

CUMMING, G., HENDERSON, R., HORSFIELD, K. & SINGHAL, S. (1969). In *The Pulmonary Circulation and Interstitial Space* (A. P. Fishman & H. A. Hecht, eds), pp. 327–340. Chicago: University of Chicago Press.

HOLLAND, P. G. (1969). *New Phytol.* **68**, 411.

HORSFIELD, K. (1967). M.D. thesis, University of Birmingham, England.

HORSFIELD, K. (1972). Ph.D. thesis, University of Birmingham, England.
HORSFIELD, K. & CUMMING, G. (1968). *J. appl. Physiol.* **24,** 383.
HORTON, R. E. (1945). *Geol. Soc. Am.* **56,** 275.
LEOPOLD, L. L. (1971). *J. theor. Biol.* **31,** 339.
MCMAHON, T. A. (1975). *Scient. Am.* **233,** 92.
MCMAHON, T. A. (1973). *Science,* **179,** 1201.
OOHATA, S. & SHIDEI, T. (1971). *Jap. J. Ecol.* **21,** 7.
PARKER, H., HORSFIELD, K. & CUMMING, G. (1971). *J. appl. Physiol.* **31,** 386.
STRAHLER, A. N. (1953). *Geol. Soc. Am.* **63,** 1117.
STRAHLER, A. N. (1964). In *Handbook of Applied Hydrology* (Van Te Chow, ed.), pp. 39–76. New York: McGraw-Hill.
WOLDENBERG, M. J. (1968). Ph.D. Dissertation, Columbia University. Federal Clearinghouse No. AD 673441.
WOLDENBERG, M. J., CUMMING, G., HARDING, K., HORSFIELD, K., PROWSE, K. & SINGHAL, S. (1972). Harvard Papers in Theoretical Geography. No. 41, Cambridge, Mass. Federal Clearinghouse No. AD 709602.

APPENDIX A

1. Tapering to insure Elastic Similarity

In Fig. 2(a) and (b), the width of the beam is $b = k_1 s^{\alpha}$, while its depth $h = k_2 s^{\beta}$. Distance along the center line from the tip is s, although actual trees do not begin until $s = l_0$ because the structure does not extend down to infinitesimal size. The overall length from the built-in end to the virtual origin is λ. In Fig. 2(c), the beam is shown leaving the trunk at arbitrary initial angle θ_0. When loaded under its own weight, the deflection of the tip is Δ. At any point s, the center line makes an angle θ with the horizontal. The small quasi-rectangular slice shaded in Fig. 2(c) is drawn large in (d), illustrating how the local radius of curvature R results in stretching the fibers in the top part of the beam and compressing the fibers in the bottom. The strain ε of fibers a distance y from the center line is

$$\varepsilon = [(R+y)\,\mathrm{d}\theta - R\,\mathrm{d}\theta]/R\,\mathrm{d}\theta = y/R. \tag{A1}$$

The local stress σ is εE, where E is the elastic modulus of the beam. Summing $\sigma\,\mathrm{d}A$ over the cross-sectional area A gives the elastic restoring moment M:

$$M = \int_A \varepsilon E y b\,\mathrm{d}y = \frac{E}{R}\int_A y^2 b\,\mathrm{d}y = \frac{EI}{R} \tag{A2}$$

where

$$I \triangleq \int_A y^2 b\,\mathrm{d}y = \frac{bh^3}{12}$$

for the rectangular cross-section. Noticing that $|R\mathrm{d}\theta| = \mathrm{d}s$, we arrive at an

equation describing the shape of the center line,

$$\frac{d\theta}{ds} = -\frac{M}{EI} \tag{A3}$$

where the minus sign accounts for the fact that θ is decreasing as s increases.

The elastic restoring moment must balance the moment M acting at a cross-section due to the weight of the beam to the right of the cross-section.

If s is the distance from the end for the cross-section under consideration, an element of weight located a distance Z from the end has a moment arm given by

$$\int_Z^s \cos\theta(\xi)\, d\xi$$

where ξ is a dummy variable of integration. The total moment is then given by the integral

$$M = \int_0^s w(Z)\, dZ \int_Z^s \cos\theta(\xi)\, d\xi \tag{A4}$$

For the beam of rectangular cross-section under consideration

$$w = \rho g b h = \rho g k_1 k_2 s^{\alpha+\beta} \tag{A2}$$

$$I = \frac{bh^3}{12} = \frac{k_1 k_2^3}{12} s^{\alpha+3\beta} \tag{A6}$$

where ρg is the weight per unit volume. Introducing the dimensionless lengths $\eta = s/\lambda$, $z = Z/\lambda$ and $\zeta = \xi/\lambda$ and substituting these along with equations (A4), (A5), and (A6) into (A3) gives:

$$\frac{d\theta}{d\eta} = -\frac{H}{\eta^{\alpha+3\beta}} \int_0^\eta z^{\alpha+\beta}\, dz \int_z^\eta \cos\theta(\zeta)\, d\zeta \tag{A7}$$

with the dimensionless coefficient

$$H = \frac{12\rho g \lambda^{-2\beta+3}}{E k_2^2} \tag{A8}$$

Equation (A7) governs the shape of the beam loaded under its own weight. It is now in dimensionless form, and therefore the shapes $\theta(\eta)$ of beams of a range of different overall lengths λ could be plotted on the same figure. The shape would in general depend on λ since H depends on λ. In the special case where $\beta = \frac{3}{2}$, H is independent of λ and all the shapes of $\theta(\eta)$ fall on the same line. This means that the tip deflection Δ is always proportional to λ, whatever value λ may take.

2. Tapering to Insure Similarity with Respect to Stress

The objective is to select the taper in such a way that the maximum stress at any cross section is independent of location along the beam. This is an extremely difficult analytic problem unless some simplification is employed. We will assume here that the beam is sufficiently stiff that only relatively small deflections take place under its own weight. (Note that stiffness and strength are entirely separate mechanical properties and a beam may fracture before very large deflections are attained.)

With small deflections, the inclination of the beam is a constant and may be taken outside of the integrals in equation (A4). Then using equation (A5) for w the integration may be performed explicitly to give

$$M = \rho g k_1 k_2 \cos\theta \frac{s^{\alpha+\beta+2}}{(\alpha+\beta+1)(\alpha+\beta+2)} = \frac{\rho g b h s^2}{(\alpha+\beta+1)(\alpha+\beta+2)} \cos\theta \qquad \text{(A9)}$$

The maximum strain at any cross section follows from (A1) if we use $h/2$ for y, and the maximum stress is E times this strain. Let σ_m denote the maximum stress:

$$\sigma_m = \frac{hE}{2R} . \qquad \text{(A10)}$$

Using equation (A2) to relate E/R to M, and then using equation (A6) for I and (A9) for M we have

$$\sigma_m = \frac{6\rho g \cos\theta}{k_2^2(\alpha+\beta+1)(\alpha+\beta+2)} s^{2-\beta}$$

To make stress independent of s, β must be 2 so that the beam depth h is proportional to s^2. Note that the maximum stress depends on α just as it depends on ρ, but a beam whose depth tapers according to $h = k_2 s^2$ has the *same* maximum stress everywhere along its length whatever the choice for α.

APPENDIX B

Natural Frequency of Power-law Beams

This topic is one which offers formidable analytic challenge unless three important simplifications are made. The first is the usual one of small amplitude vibrations, which permits the problem to be reduced to one of

linear differential equations. The second assumption is that the configuration of the beam at rest under its own weight is essentially straight (i.e., the beam is stiff in the same sense as in Appendix A, part 2). The gravitational loads and the corresponding elastic restoring moments are in equilibrium in the resting state, and when we speak of loads and moments of the vibrating system they are in addition to the static ones. The third assumption will be that the beam is close enough to being horizontal that the gravitational interaction can be neglected. For a beam which is inclined, the gravitational forces interact with and consequently influence the vibration, but for horizontal beams there is no such interaction.

From the theory of oscillations we know that the small unforced vibrations of a tapered beam can be decomposed into a sum of modal vibrations, where for each mode the structure vibrates in synchrony with a distribution of amplitude along its length known as the mode shape. The number of modes is infinite, their frequencies are generally distinct, and none of the mode shapes correspond to the static deflection under its own weight. Our interest here is with the lowest frequency (the "fundamental"). We denote by $\delta(s)$ the deflection of the beam from equilibrium at the extreme of its motion (the mode shape). Then the time varying deflection is given by $\delta(s)\cos\omega t$ where ω is the natural frequency (radians/s) of the vibration. The instantaneous acceleration of any small segment of the beam during vibration, a, is

$$a(s, t) = -\omega^2\delta(s)\cos\omega t \tag{B1}$$

and the inertial reaction force per unit length is

$$w' = a\rho bh = -\rho k_1 k_2 s^{\alpha+\beta}\omega^2\delta(s)\cos\omega t. \tag{B2}$$

From this the vibrational bending moment can be calculated as in equation (A4) with $\cos\theta$ set equal to unity

$$M' = \int_0^s (s-Z)w'(Z)\,\mathrm{d}Z. \tag{B3}$$

Since the slope of the vibrational deflection is $\mathrm{d}\delta/\mathrm{d}s$, the elastic moment equation analogous to (A3) is

$$\cos\omega t\frac{\mathrm{d}^2\delta}{\mathrm{d}s^2} = -\frac{M'}{EI} \tag{B4}$$

Combining equations (B2), (B3), (B4) and (A6) gives

$$\frac{\mathrm{d}^2\delta}{\mathrm{d}s^2} = -\frac{\int_0^s (s-Z)w'(Z)\,\mathrm{d}Z}{EI\cos\omega t} = -\frac{12\rho\omega^2\int_0^s (s-Z)Z^{\alpha+\beta}\delta(Z)\,\mathrm{d}Z}{Ek_2^2 s^{\alpha+3\beta}} \tag{B5}$$

As in Appendix A we introduce the dimensionless variables $\eta = s/\lambda$, $z = Z/\lambda$, $\delta^* = \delta/\Delta$.

$$\frac{d^2\delta^*}{d\eta^2} = -\frac{12\rho\omega^2\lambda^{4-2\beta}\int_0^\eta (\eta - z)z^{\alpha+\beta}\delta^*(z)\,dz}{Ek_2^2\eta^{\alpha+3\beta}} \tag{B6}$$

When the beam is cut off at $s = l_0 = \lambda\eta_0$, the lower limit of integration in the integral becomes η_0. The full problem, including boundary conditions, is:

$$\frac{d^2\delta^*}{d\eta^2} = -\frac{12\rho\omega^2}{Ek_2^2}\lambda^{4-2\beta}\frac{\int_{\eta_0}^\eta (\eta - z)z^{\alpha+\beta}\delta^*(z)\,dz}{\eta^{\alpha+3\beta}}$$

with

$$\frac{d^3\delta^*}{d\eta^3} = \frac{d^2\delta^*}{d\eta^2} = 0 \quad \text{at } \eta = \eta_0, \tag{B7}$$

and

$$\delta^* = \frac{d\delta^*}{d\eta} = 0 \quad \text{at } \eta = 1.$$

Each of the terms of equation (B7) is dimensionless. The coefficient of the right-hand side is the same dimensionless constant in the case of all beams:

$$\frac{12\rho\omega^2}{Ek_2^2}\lambda^{(4-2\beta)} = C. \tag{B8}$$

Solving for ω^2

$$\omega^2 = \frac{Ek_2^2 C}{12\rho\lambda^{4-2\beta}}. \tag{B9}$$

Thus in the several cases discussed in Appendix A, when:

$\beta = 0$, no taper at all, $\omega \propto 1/\lambda^2$,
$\beta = 1$, geometric similarity, $\omega \propto 1/\lambda$,
$\beta = \frac{3}{2}$, elastic similarity, $\omega \propto 1/\lambda^{\frac{1}{2}}$,
$\beta = 2$, static stress similarity, $\omega \propto \lambda^0$.

We call attention here to the fact that, in our frequency–length experiments on any particular real tree, we were keeping l_0 the same between successive frequency measurements, whereas the development above requires us to keep $\eta = l_0/\lambda$ the same. Nevertheless, it is possible to show that the constant C in equation (B8) is not very sensitive to the value of the dimensionless cutoff distance η_0. Thus one may use the length to the cutoff point l_{max} instead of the length to the virtual origin λ in the frequency–length correlations with only a small error.